A mouse model for cyclin E-dependent genetic instability and tumorigenesis

Keith R. Loeb,[1,2] Heather Kostner,[1] Eduardo Firpo,[1] Thomas Norwood,[4] Karen D. Tsuchiya,[3,8] Bruce E. Clurman,[2,3,5,*] and James M. Roberts[1,6,7]

[1]Division of Basic Sciences
[2]Division of Clinical Research
[3]Division of Human Biology
Fred Hutchinson Cancer Research Center, Seattle, Washington 98029
[4]Department of Pathology
[5]Department of Medicine
[6]Department of Biochemistry
University of Washington School of Medicine, Seattle, Washington 98109
[7]Howard Hughes Medical Institute
[8]Department of Laboratory Medicine
Children's Hospital and Regional Medical Center, Seattle, Washington 98105
*Correspondence: bclurman@fhcrc.org

Summary

Ubiquitination of murine cyclin E is triggered by phosphorylation on threonine 393. Cyclin E^{T393A} knockin mice exhibited increased cyclin E stability, but no phenotypic abnormalities. Importantly, loss of the p53 pathway exacerbated the effect of the T393A mutation. Thus, in *$p21^{-/-}$* cells the T393A mutation had an exaggerated effect on cyclin E abundance and its associated kinase activity, which caused abnormal cell cycle progression, and genetic instability involving chromosome breaks and translocations. Moreover, cyclin E^{T393A} acted synergistically with p53 deficiency to accelerate tumorigenesis in *cyclin E^{T393A} $p53^{-/-}$* mice; Ras more readily transformed *cyclin E^{T393A} $p53^{-/-}$* cells than *$p53^{-/-}$* cells in vitro; and *cyclin E^{T393A}* mice had a greatly increased susceptibility to Ras-induced lung cancer.

Introduction

Eukaryotes express regulatory proteins, called cyclins, which are required for the cell division cycle and function primarily by binding to and allosterically activating cyclin-dependent kinases (CDKs) (Sherr and Roberts, 1999). Cyclin E1 associates predominantly with one member of the CDK family, Cdk2, and serves a dual purpose in activating cell proliferation: it phosphorylates and thereby inhibits proteins that impede cell cycle progression (p27Kip1, pRb), and it phosphorylates and thereby activates proteins that promote cell division (Hwang and Clurman, 2005; Sherr and Roberts, 2004). These functions of cyclin E are essential when nondividing cells exit the quiescent state and resume cell proliferation but may be redundant with the activities of other cell cycle regulators in continuously proliferating cells (Geng et al., 2003).

Cyclin E expression and its associated kinase activity are periodic and reach a peak in early S phase (Koff et al., 1992). This periodicity is regulated by E2F-dependent cyclin E transcription (Botz et al., 1996; Geng et al., 1996; Ohtani et al., 1995) and ubiquitin-mediated cyclin E proteolysis (Clurman et al., 1996; Won and Reed, 1996). Ectopic overexpression of cyclin E causes cell cycle anomalies and genetic instability (Ohtsubo and Roberts, 1993; Spruck et al., 1999; Minella et al., 2002). It is therefore thought to be critical for normal cells to tightly regulate cyclin E activity; indeed, increased cyclin E activity is a hallmark of cancer cells.

Two ubiquitination pathways promote cyclin E degradation. Monomeric cyclin E (not bound to cdk2) is targeted by a Cullin-3 ubiquitin ligase (Singer et al., 1999). However, cyclin E that associates with Cdk2 does not interact with Cullin-3 and instead is degraded by a pathway involving the SCF^{Fbw7} ubiquitin-protein ligase (Strohmaier et al., 2001; Koepp et al., 2001; Moberg et al., 2001). Fbw7 is a bifunctional adaptor that brings phosphorylated cyclin E into proximity with the remainder of the SCF complex. At least four cyclin E phosphorylation sites regu-

SIGNIFICANCE

The abundance of cyclin E is increased in many human tumors and is predictive of tumor aggression and clinical outcome. However, it has been uncertain whether elevated cyclin E is a downstream marker for aggressive tumors or represents a driving force behind tumor progression. Our mouse model strongly supports the latter, by showing that inactivation of the normal pathway for cyclin E degradation, by direct mutation of the cyclin E gene itself, disrupts cell cycle regulation, causes genetic instability, and is, per se, oncogenic. Moreover, our mouse model shows that the impact of this misregulated cyclin E is constrained by the p53-p21 pathway, such that simultaneous loss of p53 and misregulation of cyclin E cooperate to cause oncogenic cell transformation.

late Fbw7-driven cyclin E ubiquitination; in human cyclin E these are T62, S372, T380, and S384 (Welcker et al., 2003). Most important is T380, which is phosphorylated by both GSK3 and Cdk2 itself. T380 falls within a canonical Fbw7 recognition motif, and T380 phosphorylation allows Fbw7 to bind to cyclin E (Orlicky et al., 2003; Ye et al., 2004).

Deregulated cyclin E activity is thought to play a fundamental role in tumorigenesis. A cyclin E transgene that overexpresses cyclin E induces breast carcinomas in mice, and ectopic cyclin E overexpression both induces genetic instability in cultured cells and transforms rodent fibroblasts in combination with other oncogenes (Bortner and Rosenberg, 1997; Minella et al., 2002; Spruck et al., 1999). Cyclin E containing a mutation at T380 that prevents its recognition by Fbw7 was more potent than wt-cyclin E with respect to causing cell cycle deregulation and genetic instability.

Many studies have shown that high cyclin E protein expression in human cancers is associated with increased tumor aggressiveness and poor patient outcome (Keyomarsi et al., 2002; Porter et al., 1997; Dong et al., 2000; Fukuse et al., 2000; Hwang and Clurman, 2005). In a few cancers, the cyclin E gene is amplified, but in most cases cyclin E deregulation may result from the disruption of pathways that govern its synthesis and its destruction. Fbw7 mutations have been described in cancer lines that contain high amounts of cyclin E protein as well as in primary cancers (Spruck et al., 2002; Strohmaier et al., 2001; Moberg et al., 2001; Calhoun et al., 2003). Mouse models have confirmed that Fbw7 is a tumor suppressor gene (Rajagopalan et al., 2004; Mao et al., 2004).

Although these data support a role for cyclin E in human tumorigenesis, the effects of cyclin E stabilization in general, and the specific role of cyclin E deregulation in Fbw7-associated tumorigenesis remain unclear. On the one hand, the biological effects of cyclin E stabilization have only been examined in settings that also involve ectopic cyclin E overexpression. On the other hand, Fbw7 also targets c-Myc, c-Jun, and Notch for degradation, and each of these proteins are themselves oncogenes when overexpressed (Welcker et al., 2004; Nateri et al., 2004; Wu et al., 2001). Thus, the neoplasms associated with Fbw7 loss may result from activation of any (or all) of these oncogenic targets.

Results

Targeting strategy for cyclin E^{T393A}

We constructed a knockin mouse in which the wild-type cyclin E gene was precisely replaced with one encoding a nonphosphorylatable residue, alanine, at the critical 393 position (equivalent to T380 in human cyclin E). This murine model has two important features: (1) cyclin E is resistant to Fbw7-mediated degradation but is transcribed at normal levels from its endogenous transcription unit; and (2) the role of disabled cyclin E turnover is separated from the activities of other oncogenic Fbw7 substrates caused by mutations within Fbw7 itself. We created a gene-targeting construct by using site-directed mutagenesis to change threonine 393 in exon 11 of the murine cyclin E gene to alanine, and by placing a Neo^r selectable marker flanked by LoxP sites into the intron between exons 10 and 11 and the gene encoding diphtheria toxin (DTA) upstream of exon1 (Figure 1). After transfection of embryonic stem (ES) cells and selection for G418 resistance, the precise replacement of the endogenous cyclin E gene by the cyclin E^{T393A} allele was confirmed by PCR, Southern blot hybridization, and then direct genomic DNA sequencing to demonstrate the presence of the T393A mutation (Figure 1 and data not shown). Chimeric mice that demonstrated germline transmission of the cyclin E^{T393A} allele were generated from two such ES cell clones. To eliminate the Neo^r marker, cyclin E^{T393A} mice were mated with MORE mice, in which Cre recombinase has been targeted to the Mox-2 locus and is therefore expressed early germ cells (Tallquist and Soriano, 2000). Deletion of the Neo^r gene was monitored by PCR amplification and confirmed by direct DNA sequencing (Figure 1). Mice were then backcrossed into both 129/SV and C57/Bl6 backgrounds for five generations.

Interbreeding of cyclin E^{T393A} heterozygous mice led to the recovery of all expected genotypes with normal Mendelian ratios (Figure 1D). Cyclin E^{T393A} homozygous mice were followed for 2 years; they displayed no gross phenotypic abnormalities and appeared indistinguishable from the wild-type littermates. Detailed histopathological analysis revealed normal morphogenesis in all tissues examined. The only significant abnormality was a mild to moderate splenomegaly (1–2× weight) with mild extramedullary hematopoiesis. The cyclin E^{T393A} mice displayed a normal life span with no significant predilection for hyperproliferative lesions or tumors.

Expression and activity of cyclin E^{T393A}

The effect of the cyclin E^{T393A} mutation on the expression of endogenous cyclin E, its associated kinase activity, and cell cycle regulation was studied in endogenous mouse tissues and embryonic fibroblasts (MEFs) isolated from day 12–14 embryos. The cyclin E protein was readily detected in extracts prepared from the spleen and thymus from 2- to 4-month-old mice, tissues with many proliferating cells (Figure 2A). However, the level of cyclin E and its associated kinase activity in the nonproliferative tissues from 2- to 4-month-old mice including lung, liver, and kidney was below the limit of detection (data not shown). Most strikingly, the abundance of the cyclin E protein in the splenic extracts from cyclin E^{T393A} mice consistently showed a 5- to 10-fold increase compared to age-matched wild-type controls, while a more limited 2- to 3-fold elevation in the level of cyclin E was detected in cyclin E^{T393A} thymic extracts. The amount of cyclin E-associated kinase activity closely paralleled the amount of cyclin E protein (Figure 2A). Consistent with the increase in cyclin E protein levels, freshly isolated E^{T393A} splenocytes showed a 4-fold increase in the number of cycling cells compared to matched wild-type splenocytes (Figure 2B). Histologic examination of the corresponding splenic sections, performed to rule out an occult malignancy, showed only a mild increase in extramedullary hematopoiesis. Fractionation of the spleen into populations enriched for either B or T lymphocytes showed that cyclin E^{T393A} was elevated equally in both compartments (data not shown).

A small increase in cyclin E protein abundance and its associated kinase activity (1.5–2.2×) was detected in asynchronously proliferating heterozygous and homozygous *cyclin E^{T393A}* MEFs (Figure 2C). This appeared to be due to a small increase in the half-life of cyclin E^{T393A} (5 hr) in comparison to wild-type cyclin E (4 hr), as determined both by ^{35}S pulse-

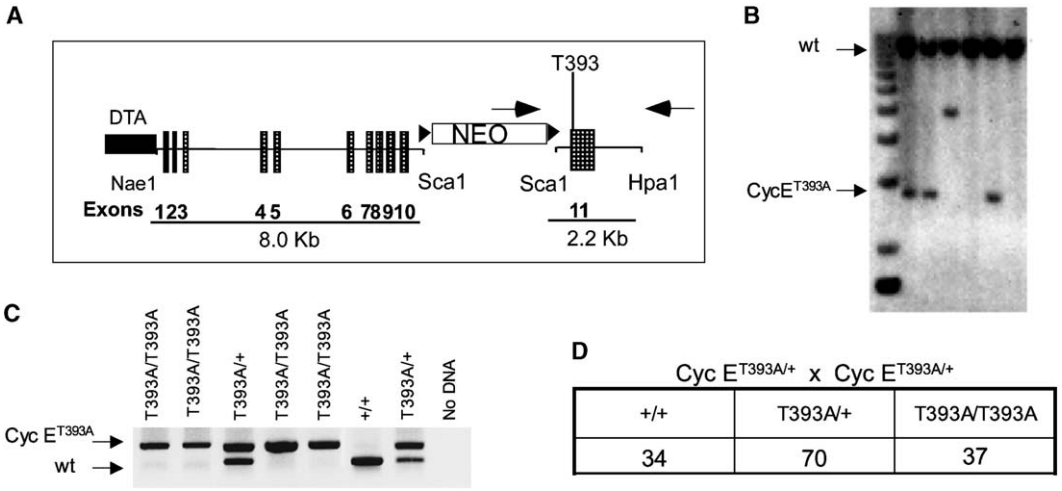

Figure 1. Construction of a cyclin E^{T393A} knockin mouse

A: The targeting construct encoding the murine cyclin E gene modified to express a cyclin E^{T393A}. Arrowheads designate LoxP sites, and arrows designate PCR primer sites. DTA, diphtheria toxin gene.

B: Southern blot of murine genomic DNA from embryonic stem cell clones selected for homologous integration of the *cyclin* E^{T393A} targeting construct. The DNA was digested with SpeI that cuts within the Neo^r gene and once downstream of the cyclin E gene, which falls outside of the targeting construct. Probe was from a murine cyclin E cDNA corresponding to exon 11. The band predicted for homologous integration of the *cyclin* E^{T393A} transgene is observed in lanes 2, 3, and 6.

C: PCR genotyping. Both wild-type and *cyclin* E^{T393A} are detected following Cre-mediated recombination. DNA with *cyclin* E^{T393A} is larger based on the presence of an additional 150 bp derived from the LoxP DNA, which are present in the terminal intron after targeting.

D: *Cyclin* E^{T393A} heterozygous matings result in the normal Mendelian ratio of expected genotypes.

chase measurement and by cycloheximide-mediated inhibition of protein synthesis (Figures 2D and 2E), whereas the amount of the cyclin E^{T393A} mRNA was unchanged compared to wild-type cyclin E (data not shown). The surprisingly small effect of the T393A mutation on cyclin E stability in MEFs is explained by the assembly of most cyclin E protein into catalytically inactive complexes with the CDK inhibitor p21Cip1, which stabilizes cyclin E through the inhibition of its associated kinase activity, and is addressed in greater detail below (Clurman et al., 1996; Welcker et al., 2003). The stability of cyclin E^{T393A} was still regulated by ubiquitin-dependent degradation, since proteasome inhibition increased the half-life of cyclin E^{T393A} from 5 hr to greater than 8 hr (data not shown). The modestly increased amount of cyclin E^{T393A} was not associated with a consistent change in the distribution of MEFs into the G1, S, or G2/M compartments of the cell cycle (data not shown).

We also examined the expression and activity of cyclin E in early passage MEFs that were synchronized by serum starvation/contact inhibition and then released into normal growth medium (Figure 3A). Note that, in contrast to similar experiments performed using human cell lines, the amount of cyclin E protein in primary MEFs was close to invariant throughout the cell cycle, with a small peak in S phase. Cyclin E-associated kinase activity was more periodic than its overall protein abundance and was limited to late G1 and S phase (Figures 3A and 3B). The cyclin E^{T393A} protein was more abundant, and its associated kinase activity was both higher and somewhat less periodic than the wild-type cyclin E protein and kinase activity. Parallel cultures were pulse labeled with BrdU and harvested for flow cytometry to determine the effect of the T393A mutation on progression through the cell cycle. In these early passage MEFs, the premature activation of cyclin E^{T393A}-associated kinase activity did not have a reproducible effect on the rate at which cells completed G1 and entered S phase (Figure 3C).

The elevated level of cyclin E^{T393A} detected in splenic extracts suggested that loss of the T393 phosphorylation might have a significant effect on lymphocyte activation and proliferation. Resting T lymphocytes expressed barely detectable levels of cyclin E. Following activation, the level of cyclin E^{T393A} increased earlier and to a greater extent than wild-type protein (Figure 3D). This resulted in an increase in the percentage of cells activated by a mitogenic stimulus (IL-2 receptor expression) and in the rate of cell proliferation (Figures 3E and 3F). These observations were consistent with the splenomegaly found in cyclin E^{T393A} mice.

Cellular immortalization enhances the effect of cyclin E^{T393A}

Cyclin E^{T393A} had a much more significant effect on cell proliferation of MEFs immortalized by a 3T3 protocol. The proliferation of control and *cyclin* E^{T393A} MEFs entered a plateau between passages 5 and 10. In most experiments, the *cyclin* E^{T393A} MEFs resumed exponential proliferation between passages 15 and 25, while the control cells frequently remained in the plateau phase until passages 25–30. A representative result is shown (Figure 4A). This escape from senescence is a stochastic process with considerable variability among genetically identical clones of fibroblasts. Nevertheless, the cyclin E^{T393A} fibroblasts typically immortalized earlier than control cells.

After immortalization, *cyclin* E^{T393A} MEFs grew faster and to

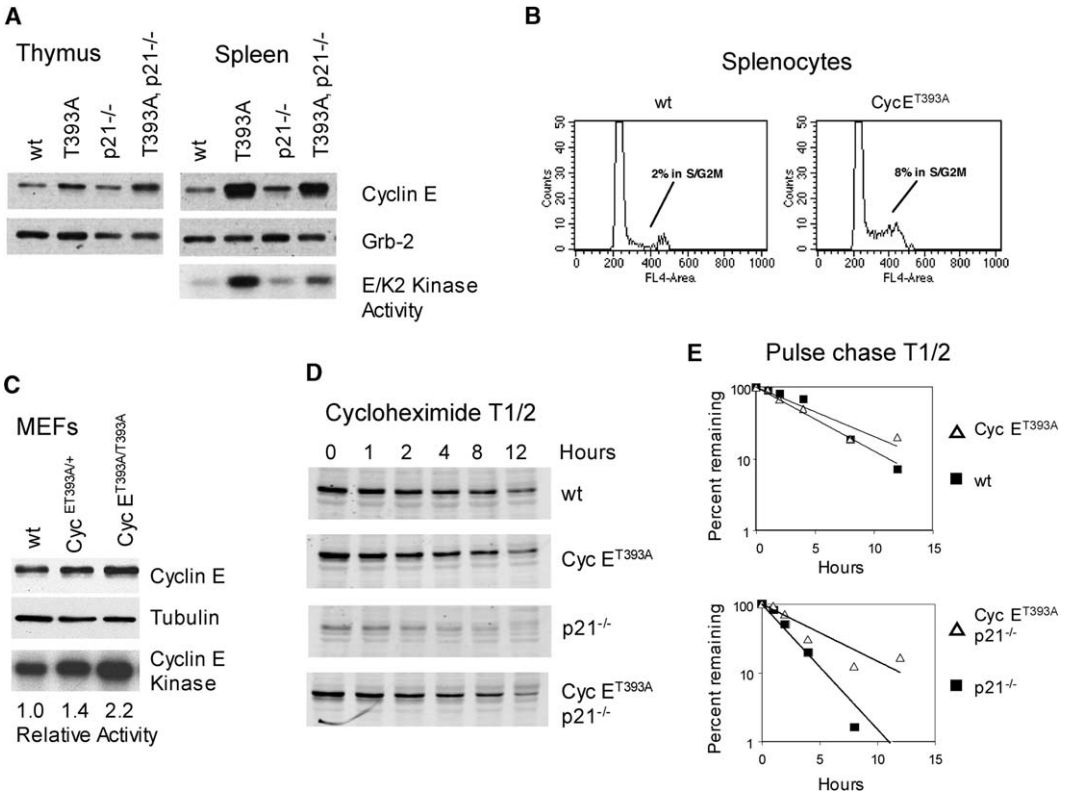

Figure 2. Analysis of cyclin E^{T393A} expression and stability in tissue and cultured fibroblasts

A: Splenic and thymic extracts from age-matched mice (8–12 weeks) of indicated genotypes were assayed for cyclin E level by Western blot. Grb-2 was used as a loading control. Cyclin E-associated kinase activity was determined from anti-cyclin E immunoprecipitation of the splenic lysate using histone H1 as substrate.

B: Expression of cyclin E^{T393A} triggers a 4-fold increase in proliferating splenocytes. Splenocytes pooled from three mice of similar ages (2–4 months) were stained with propidium iodide (PI) and analyzed by flow cytometry.

C: Asynchronously proliferating *cyclin* E^{T393A} MEFs have increased cyclin E protein and associated kinase activity. Western analysis of early passage (P2) cycling MEFs stained with anti-cyclin E antibody. Tubulin was used as loading control. Cyclin E-associated kinase activity was measured from anti-cyclin E-immunoprecipitated complexes. Kinase activity was quantified by phosphorimaging.

D: Effect of p21 on cyclin E stability. Cycloheximide half-life of cyclin E was determined by Western blot analysis of S phase-enriched MEFs. Synchronized MEFs (serum starvation) were released, grown for 20 hr, and exposed to cycloheximide for the indicated times.

E: Asynchronously proliferating MEFs were pulse labeled with ^{35}S-methionine and harvested at the indicated times. The amount of labeled cyclin E was determined by phosphorimage analysis of anti-cyclin E-immunoprecipitated extracts that had been resolved by SDS-PAGE.

a 2-fold greater saturation density (data not shown) than the immortalized control MEFs. The amount of cyclin E protein was also considerably greater in the *cyclin* E^{T393A} immortalized MEFs compared to control immortalized MEFs (Figure 4B), and this was associated with an earlier entry into S phase in synchronized cells (Figure 4C).

Interaction of cyclin E^{T393A} with the p53-p21 pathway

Our results suggested that the biological effects of cyclin E^{T393A} were being constrained in early passage cells by a factor(s) that was lost upon immortalization. One candidate was the CDK inhibitor p21Cip1, which has previously been shown to limit the effects of misregulated cyclin E in transfected cells (Minella et al., 2002). In the immortalized cells described above, p21 levels were reduced (data not shown), presumably as a secondary effect of p53 inactivation.

To investigate the role of p21 in controlling cyclin E activity, we crossed the E^{T393A} allele into a p21 null background. In most tissues, the amount of cyclin E^{T393A} and its associated kinase activity were similar in *cyclin* E^{T393A} and *cyclin* E^{T393A} $p21^{-/-}$ mice (Figure 2A). In early passage MEFs, however, the loss of p21 had a significant impact on the abundance and activity of cyclin E^{T393A} relative to wild-type cyclin E. As previously reported, cyclin E protein levels were greatly reduced in p21 null MEFs, and its half-life was reduced to 2 hr (Figures 4D, 4E, 2D, and 2E) (Welcker et al., 2003). This was thought to be caused by an increase in CDK2-dependent phosphorylation of cyclin E, and an increase in its rate of degradation by the T393-dependent pathway. Consistent with this idea, the stability and abundance of cyclin E^{T393A} was largely unaffected by the loss of p21 (Figures 4D, 4E, 2D, and 2E), and as a consequence it was both more stable (Figures 2D and 2E) and more abundant (Figures 4D and 4E) than wild-type cyclin E in the p21 null background.

The increased amount of cyclin E^{T393A} in p21 null MEFs correlated with both an increased amount of cyclin E-associ-

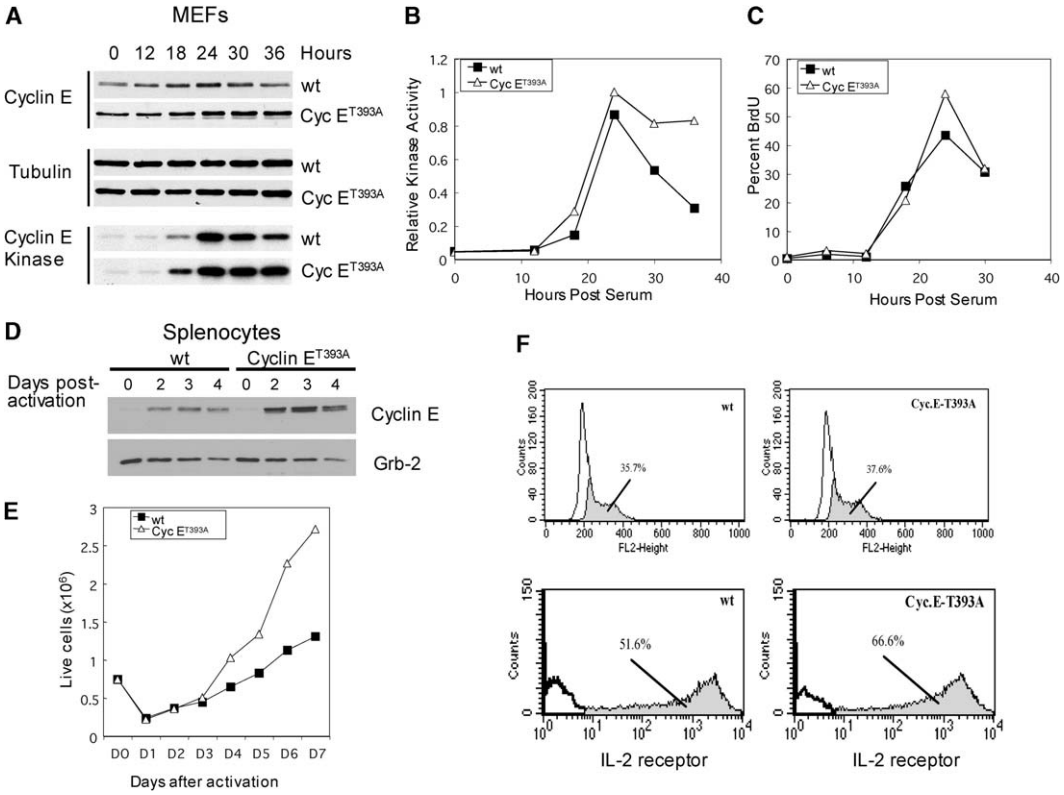

Figure 3. Effect of cyclin E^{T393A} on cell cycle regulation

A: Synchronized *cyclin* E^{T393A} and wild-type MEFs were released by serum stimulation and harvested at the indicated times. Cyclin E level was determined by Western blot analysis of cell lysates. Tubulin was used as loading control. Anti-cyclin E-immunoprecipitated extracts were assayed for kinase activity.

B: Cyclin E-associated kinase activity from **A** was quantified by phosphorimage analysis.

C: Parallel cultures of synchronized *cyclin* E^{T393A} and wild-type MEFs were released by serum stimulation and pulsed with BrdU (100 μm) for 1 hr prior to harvest. Nuclei prepared from ethanol-fixed cells were stained with anti-BrdU and PI and analyzed by flow cytometry. Percent BrdU-labeled cells was determined using CellQuest software.

D: Pooled unfractionated splenocytes (three mice per genotype) were activated with PMA-P (10 μg/ml) plus mouse recombinant IL-2 (50 ng/ml). Cells were harvested and lysed on the indicated days postactivation. Cyclin E level was determined by Western blot using Grb-2 as a loading control.

E: Enriched T cell splenocytes were activated with PMA-P and IL-2. Live cell counts were performed at the indicated times by trypan blue exclusion. Data are derived from pooled splenocytes isolated from three mice (2–4 months) for each genotype. The results are representative of those obtained from multiple independent experiments.

F: Percentage of S/G2 nuclei (upper panels) and activated T cells (lower panels). Day 3 (postactivation) growing T cells from each genotype were isolated, and nuclei were prepared and stained with PI. Parallel day 3 cells were isolated and stained with PE-fluorochrome-conjugated, anti-mouse IL-2R. Activated cell number was determined by flow cytometry using CellQuest software.

ated kinase activity (Figures 4E and 4F) and increased rate of progression from quiescence to S phase (Figure 4G). Note that the cyclin E^{T393A} $p21^{-/-}$ cells remained in S phase with a high percentage (60%) of BrdU-labeled cells at late time points, while the number of BrdU-positive $p21^{-/-}$ fibroblasts started to decline. This pattern suggested that the cyclin E^{T393A} induced both early entry into and delayed progression through S phase in a p21 null background, similar to what has been seen in cells overexpressing wild-type cyclin E (Ohtsubo and Roberts, 1993; Minella et al., 2002; Ekholm-Reed et al., 2004).

In summary, our data showed that induction of p21Cip1 could suppress the effect of the cyclin E^{T393A} mutation. When p21 expression was reduced, either indirectly during spontaneous immortalization or by direct genetic targeting, this phenotypic suppression was lost, resulting in greater cyclin E levels, higher amounts of cyclin E-associated kinase activity, and aberrant timing of S phase initiation and completion.

In contrast to cultured fibroblasts, the level of p21 in wild-type splenic extracts or resting splenocytes was undetectable prior to cell activation (data not shown). Moreover, the level of p21 expressed in activated wild-type splenocytes was 5- to 10-fold lower than that in proliferating MEFs. The preferential effect of cyclin E^{T393A} on splenocytes of wild-type mice was therefore consistent with our data showing that the consequences of this mutation were increased in p21-deficient cells.

Cyclin E misregulation causes genetic instability

Whereas cyclin E^{T393A} slightly increased the rate of proliferation of early passage control MEFs, it significantly inhibited proliferation of p21 null cells (Figures 5A and 5B). In contrast, cyclin E^{T393A} significantly increased the proliferation rate of *p53* null MEFs (*cyclin* E^{T393A} $p53^{-/-}$), thereby recapitulating the phenotype that we observed in spontaneously immortalized cells (Figure 5C). Thus, decreased p21 expression removed an in-

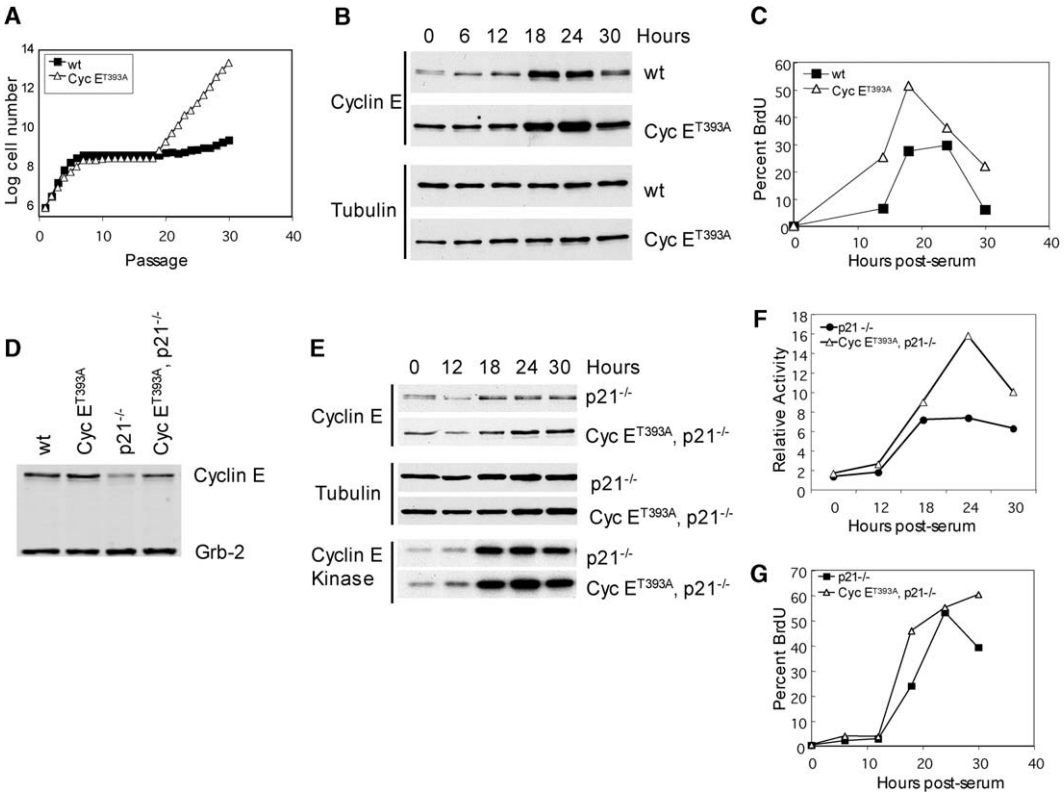

Figure 4. Effect of cyclin E^{T393A} on cycle regulation in spontaneously immortalized and p21 null MEFs

A: Growth curves of *cyclin* E^{T393A} and wild-type MEFs cultivated according to a 3T3 protocol. Total cell number was determined from cell count and dilution at each passage.

B: Spontaneous immortalized MEFs (passage 32) were synchronized by serum starvation, released into normal media, and harvested at the indicated times. Cyclin E level was determined by Western blot using tubulin as loading control.

C: Parallel cultures of synchronized immortal MEFs were pulsed with BrdU (100 μm) for 1 hr prior to harvest. Nuclei were stained with anti-BrdU and PI and analyzed by flow cytometry. The results are representative of those obtained from multiple independent experiments.

D: Western blot detection of cyclin E in asynchronously proliferating early passage MEFs of the indicated genotypes. Grb-2 is a loading control.

E: MEFs of the indicated genotypes were synchronized by serum starvation, released, and harvested at the indicated times. Cyclin E level was determined by Western blot analysis of cell lysates. Lanes were normalized for total protein and confirmed by parallel Western blots stained for tubulin. Cyclin E-associated kinase activity was measured in an anti-cyclin E immunoprecipitate kinase assay.

F: Cyclin E-associated kinase activity from **A** was measured using phosphorimage analysis.

G: Parallel cultures of synchronized MEFs were released from quiescence by serum stimulation and pulse labeled with BrdU (100 μm) for 1 hr prior to harvests. Nuclei harvested from ethanol-fixed cells were stained with anti-BrdU and PI and then analyzed by flow cytometry. The percent of BrdU-positive cells was determined by CellQuest software.

trinsic constraint on cyclin E activity, but this was associated with enhanced cell proliferation only if p53 was inactive.

We next looked at long-term growth and senescence in a 3T3 protocol (Figure 5D). p21 null MEFs underwent a very transient senescence with minimal morphologic changes. In contrast, p21 null cells expressing cyclin E^{T393A} showed a pronounced defect in proliferation rate and grossly altered cell morphology, from which they did not recover for at least 15 passages.

The slow growth of *cyclin* E^{T393A} $p21^{-/-}$ MEFs was associated with the accumulation of DNA damage. Phosphorylation of p53 on serine 15 is a sensitive indicator of DNA damage (Giaccia and Kastan, 1998). Asynchronously proliferating *cyclin* E^{T393A} *p21* null fibroblasts had an elevated amount of serine 15-phosphorylated p53 compared to p21 null fibroblasts (Figure 5E, compare lanes 1 and 3). Following irradiation, the level of p53 phosphorylated on serine 15 was elevated to a similar extent in both genotypes (Figure 5E, compare lanes 2 and 4). Using synchronized cells, we found that p53 serine 15 phosphorylation occurred in late S phase, with a slightly earlier appearance and increased abundance of p53 phosphorylation in the *cyclin* E^{T393A} $p21^{-/-}$ MEFs (data not shown). The increased spontaneous phosphorylation of p53 was dependent on the absence of p21, because the amount of serine 15-phosphorylated p53 in *cyclin* E^{T393A} cells was very low and comparable to that of control MEFs (data not shown). This was consistent with our other observations showing that the abnormal activity associated with cyclin E^{T393A} was constrained by p21.

The slowing of S phase progression and the induction of the p53 response suggested that cyclin E^{T393A} might be inducing DNA damage. Direct evidence for cyclin E^{T393A}-dependent genetic instability emerged from flow cytometric and cytogenetic analyses. At early passages, there were an increased number of *cyclin* E^{T393A} $p21^{-/-}$ cells with a tetraploid DNA content,

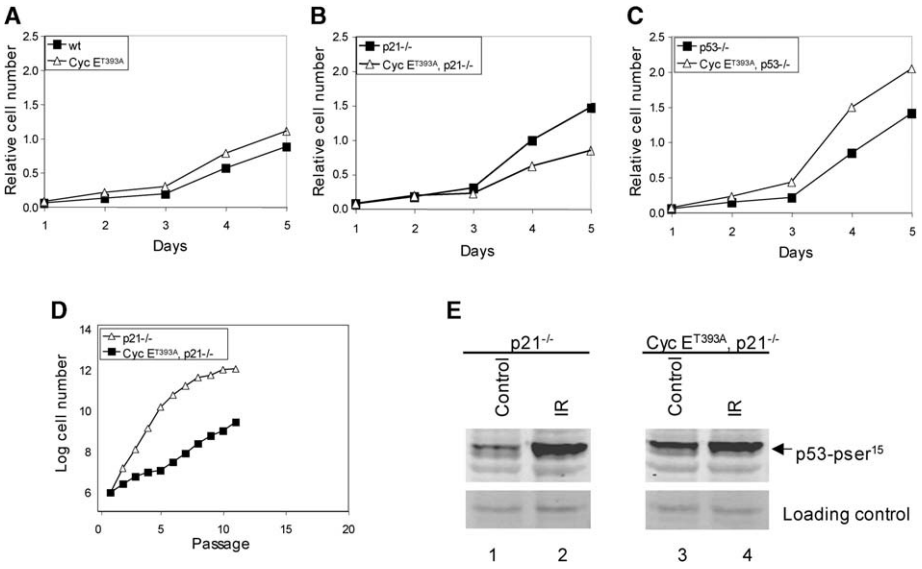

Figure 5. Expression of cyclin E^{T393A} in p21 null MEFs inhibits cell growth

A–C: Short-term growth curves of MEFs of the indicated genotypes.

D: Growth curve of *cyclin* E^{T393A} $p21^{-/-}$ and $p21^{-/-}$ MEFs cultivated according to a 3T3 protocol. Total cell number was determined from cell count and dilution at each passage. The data represent a single experiment that has been repeated several times with different MEF isolates.

E: Western blot of p53 phosphorylated on serine 15 in asynchronously proliferating cultures of *p21 cyclin* E^{T393A} $p21^{-/-}$ (lanes 1 and 2) and *cyclin* E^{T393A} $p21^{-/-}$ MEFs (lanes 3 and 4) that were either mock irradiated (lanes 1 and 3) or irradiated (lanes 2 and 4). Irradiated cell were harvested 24 hr after exposure to 10 Gy.

while at later passages an aneuploid population accumulated (Figure 6A). In comparison, parallel cultures of p21 null fibroblasts were stably diploid. To expand these findings, we performed cytogenetic studies on midpassage MEFs (passage 4 and 14), which showed that cyclin E^{T393A} caused the accumulation of a plethora of unstable chromosomal aberrations defined as chromatid/chromosome breaks, gaps, and radial figures in both p21 null and p53 null backgrounds (Figures 6B and 6C and Table S1). The presence of stable karyotypic abnormalities in cells expressing cyclin E^{T393A} was confirmed by spectral karyotyping (SKY) analyses (Figure 6D). These data are consistent with the findings that ectopic cyclin E overexpression induces genetic instability in primary human cells only after disruption of the p53-p21 pathway (Minella et al., 2002).

Cyclin E^{T393A} is an oncogene

That fact that cyclin E^{T393A} could promote genetic instability in vitro suggested that the mutation might be oncogenic. As an initial test of this hypothesis, we scored the ability of cyclin E^{T393A} to cooperate with activated H-Ras^{G12V} and p53 deficiency to promote the formation of transformed cell foci in vitro. Transfection of p53 null MEFs with activated *H-*Ras^{G12V} resulted in the appearance of multiple foci of transformed cells after 2–3 weeks of growth in culture. Strikingly, the p53 null MEFs expressing E^{T393A} were hyperresponsive to transformation by activated H-Ras (Figure 7A). Transfection efficiencies were comparable, since parallel control cells transfected with β-galactosidase showed similar transfection efficiency in both p53 null cell lines (data not shown). Stable expression of activated H-Ras in p53 null MEFs expressing E^{T393A} produced a striking morphologic change with abundant rounded cells (Figure 7B) and a 3-fold increase in mitotic figures (data not shown). The *H-*Ras^{G12V} $p53^{-/-}$ *cyclin* E^{T393A} cells exhibited only a small increase in proliferation rate compared to cells expressing wild-type cyclin E (Figure 7C) but had a saturation density at confluence that was 2- to 4-fold greater (Figure 7E). Parallel cytogenetic studies showed a large (2- to 3-fold) increase in chromosomal aberrations in the cells expressing cyclin E^{T393A} when compared to *H-*Ras^{G12V} $p53^{-/-}$ MEFs expressing wild-type cyclin E (Figure 7D). The number of radial figures and chromatid breaks were selectively elevated. Thus, the transforming effect of cyclin E^{T393A} was reflected in its ability to induce genetic instability and its effects on cell proliferation.

To extend these in vitro results to in vivo models of tumorigenesis, we investigated the ability of cyclin E^{T393A} to promote tumorigenesis both in p53 null mice and in mice expressing activated Ras. We found that cyclin E^{T393A} caused a statistically significant acceleration of tumorigenesis in the already highly tumor-prone p53 null background ($p = 0.05$). Thus, *cyclin* E^{T393A} $p53^{-/-}$ mice had a mean tumor-free survival of 145 days compared to 180 days in p53 null mice (Figure 8A). This acceleration of tumorigenesis was comparable to the effect observed when p53 deficiency was combined with p27 deficiency (Philipp-Staheli et al., 2004). There was no difference in the spectrum of tumors that developed in $p53^{-/-}$ versus *cyclin* E^{T393A} $p53^{-/-}$ mice.

As a further test of its ability to promote oncogenic transformation and promote genetic instability in vivo, we introduced the cyclin E^{T393A} allele into mice that harbored a latent, spontaneously activated allele of activated K-Ras^{G12D} (Johnson et al., 2001). Expression of activated K-Ras results in the development of multiple lung adenomas and adenocarcinomas with near 100% penetrance. Expression of the cyclin E^{T393A} mutation in conjunction with activated K-Ras resulted in a dramatic increase in tumor-associated mortality with a mean survival of just 160 days compared to 260 days with activated K-Ras alone (Figure 8B). The expression of cyclin E^{T393A} did not affect tumor morphology; the tumors varied from low-grade adenomas to adenocarcinomas with focal areas of moderate to high-grade dysplasia (Figure 8C). Young mice harvested between 2 and 4 months showed multiple tumors with a trend toward a higher number of foci in the mice expressing cyclin E^{T393A}. The tumor burden in advanced-stage mice was difficult to determine because of tumor coalescence. Figure 8C shows representative examples of lungs harvested from 7-month-old

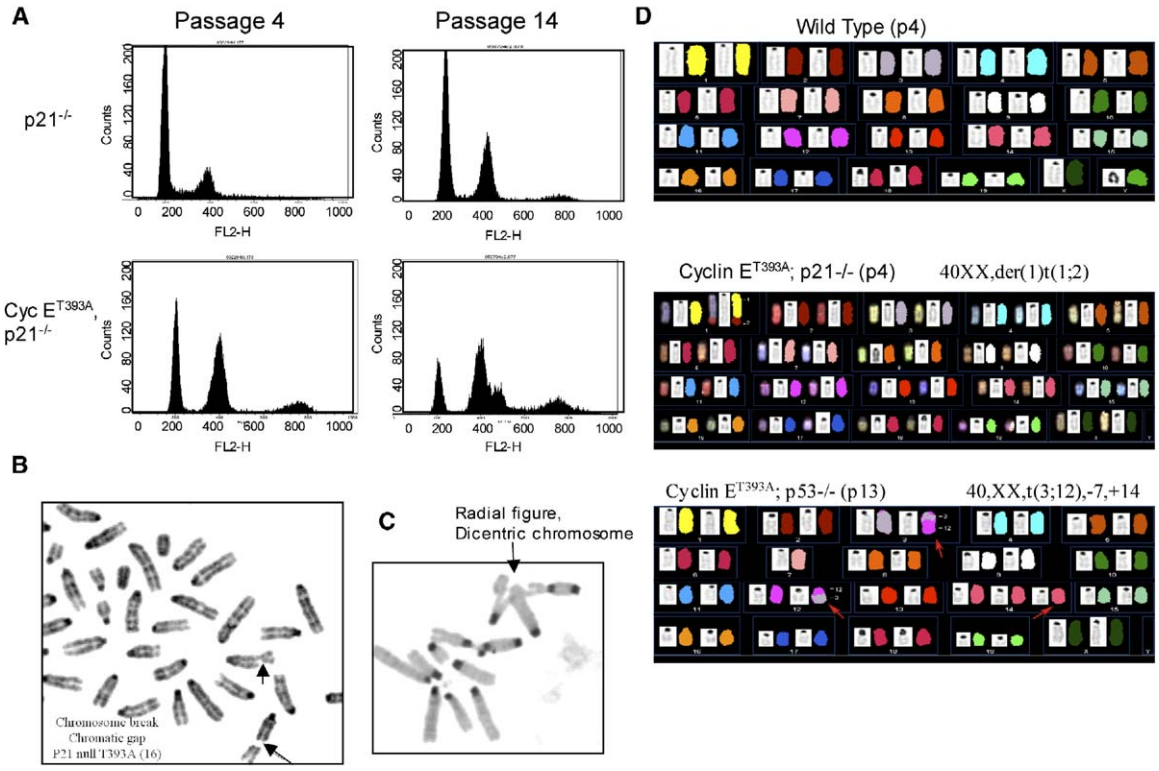

Figure 6. Cyclin E^{T393A} expression in *p21* null MEFs triggers genomic instability

A: Cell cycle profiles of early (P4) and late (P14) *cyclin* E^{T393A} $p21^{-/-}$ and $p21^{-/-}$ MEFs.
B: Metaphase spread of late passage (p16) *cyclin* E^{T393A} $p21^{-/-}$ MEFs (unbanded) showing a representative chromosome break and gap (arrows).
C: Metaphase spread of late passage (p16) *cyclin* E^{T393A} $p21^{-/-}$ MEFs (C banding stain) showing a radial figure and dicentric chromosome (arrow).
D: Spectral karyotyping analysis (SKY) of early passage (p4) wild-type and *cyclin* E^{T393A} $p21^{-/-}$ and late passage (p13) *cyclin* E^{T393A} $p53^{-/-}$ MEFs. Representative chromosome rearrangements detected in cells expressing cyclin E^{T393A} are shown.

K-Ras^{G12D} mice expressing wild-type cyclin E and cyclin E^{T393A}.

To determine the effect of cyclin E^{T393A} on genetic instability during tumorigenesis, in vivo tumors from age-matched animals were analyzed by array-based comparative genomic hybridization (array CGH). Two of six *cyclin* E^{T393A} *K-ras*^{G12D} tumors showed significant gains and losses of whole chromosomes (Figure 8D). A third cyclin E^{T393A} tumor also showed evidence of chromosome instability, but chromosome gains and loses in this tumor were less prominent (data not shown), perhaps due to clonal heterogeneity or contaminating nonneoplastic cells. In contrast, no chromosome changes were detected in any of the five *K-ras*^{G12D}, *wild-type cyclin E* tumors we analyzed.

Discussion

The key question we address in these studies is whether targeted misregulation of the murine cyclin E protein expressed from its endogenous locus is sufficient to cause abnormal cell cycle progression and genetic instability and promote oncogenic cell transformation. Previous studies have shown that increased amounts of cyclin E can cause cell cycle abnormalities and induce tumorigenesis. However, this conclusion was based on ectopic overexpression studies in cell culture and transgenic mouse models, both of which involve the analysis of cyclin E levels that vastly exceed the amount expressed in a normal cell. This idea also emerged from the complex phenotype associated with inactivation or reduced expression of the Fbw7 gene product, a protein that plays a critical role in cyclin E ubiquitination and degradation. In fact, Fbw7 is mutated in several epithelial cancers including breast, ovary, pancreatic, and endometrial carcinoma (Spruck et al., 2002; Strohmaier et al., 2001; Moberg et al., 2001; Calhoun et al., 2003). However, in addition to cyclin E other regulatory proteins are ubiquitinated by Fbw7, including Notch, Myc, and Jun, all of which have been implicated in tumorigenesis. Therefore, the phenotype caused by Fbw7 mutations may depend on its effects on several downstream effectors.

To circumvent these ambiguities, and to directly examine the consequences of cyclin E misregulation, we have taken the approach of specifically disrupting the normal degradation of cyclin E by the ubiquitin-proteasome system, by constructing a mouse model in which the wild-type cyclin E gene is precisely replaced with one encoding alanine instead of threonine at position 393. Our results show that this single amino acid change is sufficient to stabilize cyclin E, and in some settings to induce cell cycle misregulation, genetic instability, and tumorigenesis. The magnitudes of these effects are highly tissue specific, and in many cell types this mutation has only minor consequences.

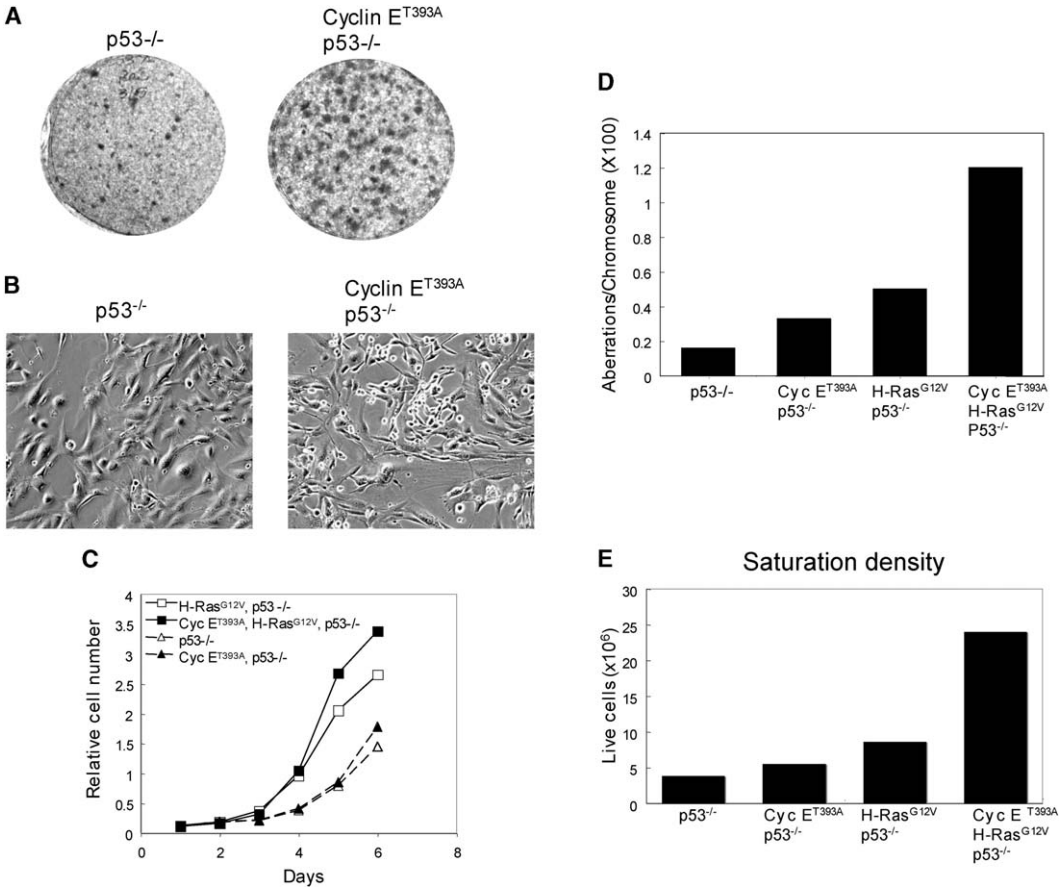

Figure 7. Cyclin E^{T393A} promotes H-Ras^{G12V}-mediated transformation

A: Focus formation by *cyclin E^{T393A} p53$^{-/-}$* and *p53$^{-/-}$* MEFs that had been transfected with activated *H-Ras^{G12V}*. Foci were visualized by staining cells with crystal violet.

B: Early passage *p53$^{-/-}$* MEFs expressing wild-type or cyclin E^{T393A} were infected with retrovirus encoding activated *H-Ras^{G12V}*. Image is a phase contrast micrograph (200×) showing a large number of refractory and rounded cells expressing cyclin E^{T393A}.

C: Short-term growth curve of *H-Ras^{G12V}*-infected MEFs of the indicated genotypes.

D: C banded metaphase spreads from exponentially growing early passage MEFs (P7) of the indicated genotypes were screened for unstable chromosome aberrations as described above. Data are derived from analysis of 45 to 70 cells per genotype and are expressed as aberrations per chromosome because of the large number of tetraploid cells. Cells undergoing mitotic catastrophe with numerous aberrations were excluded from the analysis.

E: Early passage MEFs of the indicated genotypes were plated at 1 × 10^6 cells per 10 cm plate. Cells were grown for 10 days with fresh media every third day. Day 10 cell count was determined by trypan blue exclusion. The data represent a single experiment that has been repeated several times with similar results.

For example, T393A mutation causes a 5- to 10-fold increase in cyclin E abundance in the spleen but only a 2-fold increase in the thymus and MEFs. In MEFs, this modest effect of the cyclin E^{T393A} mutation on cyclin E protein level correlates with a similarly small effect on cyclin E stability and essentially no effect on cell cycle progression, whereas a more substantial effect on cell proliferation is evident in splenocytes. Our data indicate that this could be explained by the relative paucity of p21 in resting or activated splenocytes, and hence the differential activity of cyclin E^{T393A} in these compared to other cells.

Overall, the endogenous expression of cyclin E^{T393A} by itself has very little impact on mouse physiology or cell cycle regulation. *Cyclin E^{T393A}* mice live a normal life span with no significant spontaneous tumors or hyperproliferative lesions. Therefore, under ordinary circumstances the T393-dependent degradation pathway contributes minimally to cell cycle regulation. These results raise the question of whether the tumor-prone phenotype of Fbw7 mutant mice (Mao et al., 2004) is due to its effects on cyclin E alone. Nevertheless, in some biological contexts this pathway is crucial. For example, in certain genetic backgrounds or in response to physiological stresses (e.g., pregnancy) *cyclin E^{T393A}* mice had a high incidence of massive splenomegaly, in which the spleens increased 10- to 20-fold their normal size in conjunction with exuberant extramedullary hematopoiesis (unpublished data). Moreover, splenic extracts from these mice had enormously elevated amounts of cyclin E and associated kinase activity. The specific factors that triggered this phenotype are not yet known, but it nonetheless illustrates the precarious state of cell cycle regulation when this pathway for cyclin E degradation absent.

The interaction between cyclin E^{T393A} and the p53-p21 path-

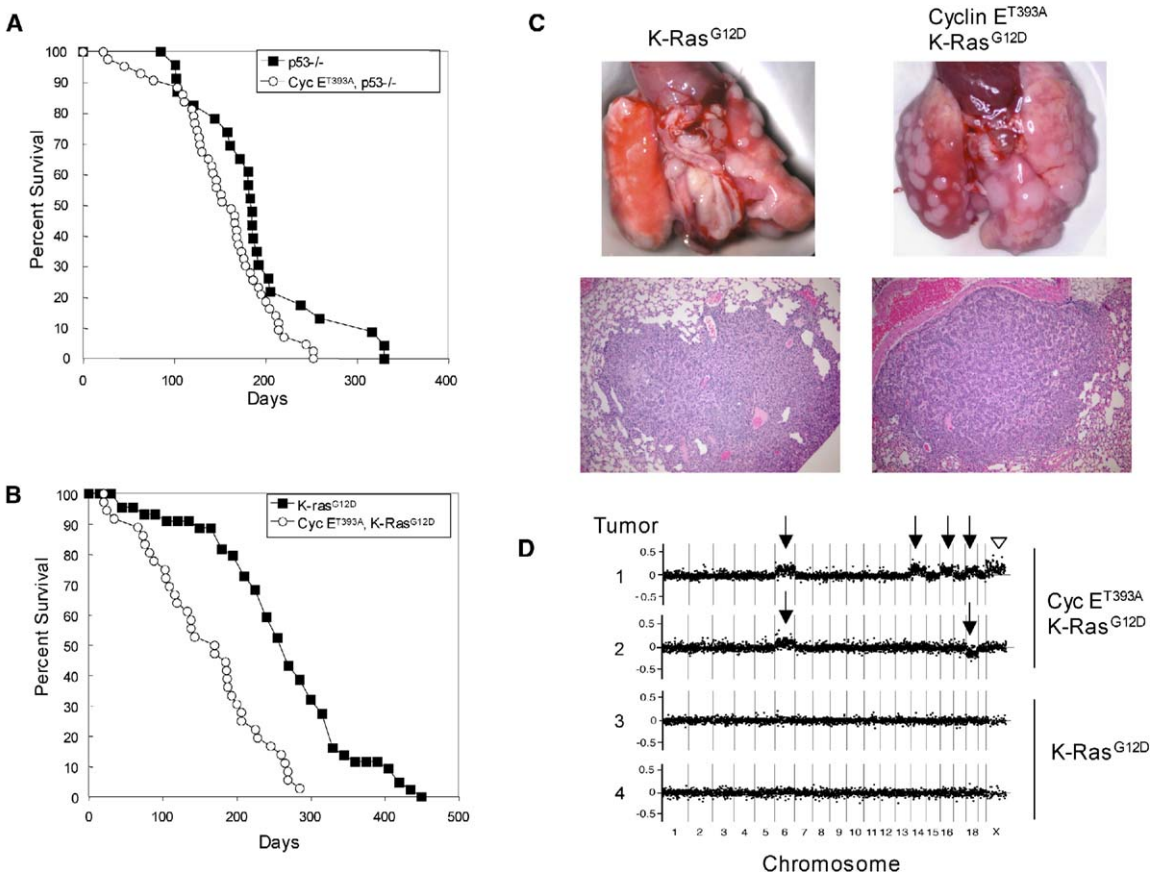

Figure 8. Cyclin E^{T393A} promotes tumor growth and genetic instability in vivo

A: Kaplan-Meier survival curve of *cyclin* E^{T393A} $p53^{-/-}$ and $p53^{-/-}$ mice. The median time of survival was 145 days for *cyclin* E^{T393A} $p53^{-/-}$ and 180 days for $p53^{-/-}$ mice. The entire cohort of 43 *cyclin* E^{T393A} $p53^{-/-}$ mice and 23 $p53^{-/-}$ mice were monitored for tumor morbidity or spontaneous death over a period of 2 years. Tumors were confirmed by histopathological analysis. Log rank test analysis showed a significant difference between the survival time of *cyclin* E^{T393A} $p53^{-/-}$ and $p53^{-/-}$ ($p = 0.05$). Both genotypes were backcrossed for greater than five generations into C57BL/6 background.

B: Kaplan-Meier survival curve of *cyclin* E^{T393A} *K-*Ras^{G12D} and *K-*Ras^{G12D} mice. The median time of survival was 160 days for *cyclin* E^{T393A} *K-*Ras^{G12D} and 260 days for *K-*Ras^{G12D} mice. The entire cohort of 36 *cyclin* E^{T393A} *K-*Ras^{G12D} and 44 *K-*Ras^{G12D} were monitored for tumor morbidity, respiratory distress, and spontaneous death over a period of 2 years. Lung tumors were confirmed by histopathological analysis. All mice died of respiratory insufficiency caused by lung tumor burden. Both genotypes were backcrossed into a pure 129/SJ background.

C: Examples of macroscopic and hematoxylin and eosin (H&E)-stained cross-sections of lung tumors found in *K-*Ras^{G12D} and cyclin E^{T393A} *K-*Ras^{G12D} mice. The macroscopic images show the entire lung with attached heart (top) isolated from age-matched mice (7 months). The tumors appear as pale white nodules on the pleural surface. The microscopic sections (lower panels) show two representative tumor nodules with focal areas of organoid morphology and focal dysplasia. Magnification, 200×.

D: Array CGH results for representative lung neoplasms from *cyclin* E^{T393A} *K-*Ras^{G12D} (tumors 1 and 2) and *K-*Ras^{G12D} mice (tumors 3 and 4). The normalized $\log_2$ ratio of fluorescence intensity in tumor versus normal reference DNA is on the y axis, and chromosome identification is shown on the x axis at the bottom. *Cyclin* E^{T393A} *K-*Ras^{G12D} neoplasms demonstrate whole chromosome gains or losses, consisting of gains of chromosomes 6, 14, 16, and 18 in one tumor (tumor 1, arrows), and gain of chromosome 6 and loss of chromosome 18 in another tumor (tumor 2, arrows). Gain of the X chromosome due to sex mismatch between one of the tumors and normal 129 male reference DNA serves as an internal control (tumor 1, arrowhead). In contrast, no definite chromosomal gains or losses are seen in neoplasms from *K-*Ras^{G12D} mice (tumor 3 and tumor 4).

way of CDK inhibition and cell cycle regulation points to another setting where normal cyclin E degradation becomes essential. Our data showed that loss of the p53-p21 pathway cooperated with the cyclin E^{T393A} mutation to severely affect cell proliferation and promote cell transformation. An interaction between these pathways was first observed in cultured cells ectopically overexpressing wild-type cyclin E or cyclin E^{T393A} (Minella et al., 2002) and was reinforced by our observations on the phenotypes of spontaneously immortalized *cyclin* E^{T393A} MEFs, which most often involve p53 inactivation and p21 downregulation. Immortalized cyclin E^{T393A} MEFs had a substantially higher level of cyclin E than did control MEFs, and this was associated with increased cell proliferation, growth to higher cell density, and early transit into S phase. The rate of immortalization was also increased by the cyclin E^{T393A} mutation. We have not yet determined whether this was due to an increased rate of p53 inactivation, although this seems likely. Therefore, not only did the loss of the p53-p21 pathway increase the effect of the T393A mutation, but this mutation may have a sufficient destabilizing effect on its own to promote p53 inactivation. Hence, these two oncogenic pathways were mutually reinforcing.

To address more directly whether the increased impact of the cyclin E^{T393A} mutation on immortalized cells was linked to loss of the p53-p21 pathway, we crossed the *cyclin E^{T393A}* allele into p53 and p21 null backgrounds. Similarly to what we observed in immortalized cells, cyclin E^{T393A} was significantly more stable, expressed at a higher steady-state level, and had a greater amount of associated kinase activity than wild-type cyclin E in the p21 null background. Moreover, these changes were associated with an early entry into and delayed exit from S phase. Unlike immortalized MEFs, however, the *cyclin E^{T393A} p21$^{-/-}$* MEFs had a severe proliferation defect, which was evident both in short-term proliferation assays and in longer-term propagation by a 3T3 protocol. This correlated with activation of the p53 DNA damage response and the onset of significant genetic instability that was manifest by the accumulation of both unstable and stable chromosome aberrations. Thus, p21 limited the activity of the deregulated cyclin E and thereby safeguarded against the effects it can have on the cell division cycle. Note that cyclin E^{T393A}-associated kinase activity was elevated both in wild-type and in p21 null MEFs, yet its deleterious affects on cell proliferation and chromosome stability were evident only in the latter. Therefore, a function of p21 in this setting was not just to limit the activity of cyclin E per se, but also to indirectly control its downstream effects on cell cycle progression. We suggest that this was due to its ability to prevent premature activation of other cell cycle kinases, including cyclin A-Cdk2 and cyclin A-Cdc2, in the face of increased and prematurely active cyclin E.

In contrast to the deleterious effects of cyclin E^{T393A} in *p21$^{-/-}$* MEFs, the *cyclin E^{T393A} p21$^{-/-}$* mice developed normally. This difference is probably attributable to the ongoing DNA damage that is present in cultured MEFs. MEFs growing in normal tissue culture conditions with 20% oxygen accumulate extensive oxygen-mediated genetic damage that limits their replicative life span, and respond to the oxygen damage through the activation of p53 that triggers the expression of p21 and cellular senescence (Parrinello et al., 2003). Therefore, conditions that induce the p53-p21 pathway are likely to be settings in which the regulation of cyclin E by the T393 pathway is particularly critical. In other words, under conditions of cellular stress, loss of this pathway together with loss of p21 will result in severe cell cycle abnormalities. Thus, exposure to genotoxic agents or irradiation may uncover a tumor-prone phenotype in *cyclin E^{T393A} p21$^{-/-}$* mice.

In a p53 null background, the effects of cyclin E^{T393A} on cell proliferation and genetic instability were evident, but its deleterious effect on cell proliferation was lost. This recapitulated the phenotype that we observed in spontaneously immortalized *cyclin E^{T393A}* MEFs. The ability of cyclin E^{T393A} to both increase cell proliferation and increase genetic instability, albeit in specific genetic backgrounds, suggested that this mutation had the potential to be oncogenic. We confirmed this hypothesis in three ways. First, *cyclin E^{T393A} p53$^{-/-}$* MEFs were much more susceptible to H-Ras-induced transformation in vitro than were *p53$^{-/-}$* MEFs expressing wild-type cyclin E. This was associated with a significant increase in genetic instability, with a morphologic phenotype typical of highly transformed cells, and with growth to a higher saturation density. Second, mice that somatically activated a *K-Ras^{G12D}* allele showed an increased rate of tumorigenesis if they also expressed cyclin E^{T393A}, with many of these tumors showing increased genetic instability by array CGH. Third, expression of cyclin E^{T393A} in *p53$^{-/-}$* mice resulted in a significantly increased rate of tumorigenesis.

Cyclin E activity is controlled at multiple levels that include gene transcription, at least two pathways of ubiquitin-dependent proteolysis, interactions with CDK inhibitory proteins, and regulatory phosphorylation on its CDK2 catalytic subunit. An important hypothesis that emerges from our studies is that misregulation of one pathway alone may not be sufficient for cyclin E to become oncogenic. In the particular example reported here, the ability of cyclin E to induce cell cycle abnormalities and genetic instability was greatly increased when the T393A stabilizing mutation was combined with loss of the p53-p21 pathway of CDK inhibition. If only a single pathway is mutated, then this may be compensated for by the activity of the other. That is, loss of p53-p21 promotes cyclin E turnover through the Fbw7 pathway by increasing the catalytic activity of cyclin E-cdk2. Conversely, if Fbw7-mediated degradation is disrupted, then p53 and p21 restrict the activity of cyclin E-cdk2. Thus, disruption of both the p53-p21 and Fbw7 pathways were necessary for cyclin E-cdk2 activity to reach oncogenic levels. It will therefore be important to determine if lesions in the other cyclin E regulatory pathways can similarly combine to induce oncogenic cell transformation.

Experimental procedures

Antibodies

Antibodies were obtained from the following sources: affinity-purified polyclonal anti-cyclin E (Clurman et al., 1996); monoclonal anti-Grb-2 (PharMingen); polyclonal anti-phospho-p53 (Ser15) (Cell Signaling); and monoclonal anti-α-tubulin (Sigma).

Mice

The targeting vector for *cyclin E^{T393A}* mice was generated from a genomic clone encoding cyclin E1 (provided by P. Sicinski). See the Supplemental Data available with this article online for details on vector construction and primers. The targeting construct was linearized and electroporated into mouse XY AK7 ES cells, and homologous recombinants were selected in G418 (Gibco). Colonies were screened by PCR amplification and confirmed by Southern blot hybridization. Two ES cell clones were used for blastocyst injection of C57/B6J mouse embryos. Germline transmission was identified in male chimaeras by PCR. The LoxP Neo cassette was excised by crossing with Cre-expressing MORE mice (provided by P. Soriano). *Cyclin E^{T393A}* mice were backcrossed for greater than five generations into c57/Bl6 and SJ129 backgrounds. *Cyclin E^{T393A}* heterozygous mice were bred with heterozygous *p21$^{+/-}$* (provided by P. Leder) (Deng et al., 1995) and *p53$^{+/-}$* mice (B6.129S2-Trp53^{tm1Tyj}; Jackson Labs) in a pure C57Bl/6J background. *Cyclin E^{T393A}* mice were crossed with LA-2 mice (provided by T. Jacks) (Johnson et al., 2001) in pure SJ129 background. Mice were aged until moribund (up to 24 months). Statistical analysis of the Kaplan-Meier survival curves was performed using log rank test.

Preparation of MEFs and tissue culture

Early passage primary MEFs were prepared as described (Malek et al., 2001). Immortalized cells were passaged on a 3T3 protocol (Todaro and Green, 1963) multiple times on independent derivatives of MEFs. Short-term cell growth assays were performed in triplicate as previously described (Smith et al., 2003). Cell synchronization and cell cycle analyses were performed with serum-starved/contact-inhibited cells as previously described (Malek et al., 2001). Cell and tissue lysates and Western blots were performed as previously described (Besson et al., 2004). Cyclin E-associated kinase activity was measured as previously described (Firpo et al., 1994).

Unfractionated and T cell-enriched splenocytes (R&D T cell enrichment columns) were isolated from the spleens of age-matched mice (2–4 months) and cultured as previously described (Firpo et al., 1994). Activation was determined by expression of transferrin receptor (FITC-TfR; BD Immuno-

chemicals) and IL-2 receptor (PE-anti-CD25; BD Immunochemicals) by flow cytometry using CellQuest software.

Activated H-Ras^{G12V} was transfected into MEFs with Fugene 6 (Roche), together with a plasmid encoding *CMV* β-*galactoside* as control. Foci formation was detected by crystal violet in plates cultured for 2 weeks. A parallel plate was assayed for β-galactosidase-positive cells. MEFs stably expressing activated H-Ras^{G12V} were generated by retroviral transduction as previously described (Besson et al., 2004).

Cyclin E half-life determination was performed by both ^{35}S-methionine pulse labeling as described (Welcker et al., 2003) and cycloheximide (25 μg/ml) treatment. Proteasome inhibition was performed by treatment with MG-132 (100 μm; Calbiochem) for 6 hr or with β-lactone (10 mM; Calbiochem).

Cytogenetic and SKY studies

Exponentially growing MEFs were treated with colcemid (0.1 μg/ml; Sigma) for 25 min and harvested by trypsinization. Cell pellets were resuspended in hypotonic buffer (0.3% KCl, 0.1% sodium citrate) and incubated 22 min at 37°C. Cells were fixed with 0.5 ml Carnoy's fixative (75% methanol, 25% glacial acetic acid), pelleted, and resuspended into 5 ml Carnoy's fixative. Fixed cells were dropped onto slides, air dried, and G banded (Seabright, 1971) or C banded (Salamanca and Armendares, 1974). The banded and unbanded preparations were stained with Wright's stain. Chromosome preparations were also hybridized with the SKY probe mixture from Applied Spectral Imaging (ASI; Magdal Haemak, Israel) for 24 hr at 37°C according to the manufacturer's protocol. Following hybridization, the preparations were counterstained with 4′,6-diamino-2-phenylindole (DAPI). The analysis was carried out using a SpectraCubeSD 300 system supported by 1.2 visualization and analysis software.

Array CGH

Mouse bacterial artificial chromosome (BAC) arrays providing a 1 Mb resolution were produced by the Genomics Shared Resource, Fred Hutchinson Cancer Research Center (FHCRC), as described (Loo et al., 2004). The mouse BAC clone set was provided by A. Bradley, Wellcome Trust Sanger Institute (Chung et al., 2004). Labeling of tumor and reference DNA (129 male) with Cy3 or Cy5, hybridization to BAC arrays, scanning, and data analysis were performed as described (Loo et al., 2004).

Supplemental data

The Supplemental Data include Experimental Procedures and one table and can be found with this article online at http://www.cancercell.org/cgi/content/full/8/1/35/DC1/.

Acknowledgments

We thank members of the Roberts and Clurman labs for helpful comments and discussion; Cassandra Neal of the FHCRC genomics resource for help with array CGH; and Shauna Pyott of the Cytogenetics lab at the University of Washington. J.M.R. is an Investigator of the Howard Hughes Medical Institute. This work was supported by NIH grants R01CA84069 (B.E.C.), R01CA102742 (B.E.C.), and NIEHS-K08-ES00382 (K.R.L.). B.E.C. is a W.M. Keck Distinguished Young Scholar in Medical Research.

Received: December 20, 2004
Revised: May 16, 2005
Accepted: June 22, 2005
Published: July 18, 2005

References

Besson, A., Gurian-West, M., Schmidt, A., Hall, A., and Roberts, J.M. (2004). p27Kip1 modulates cell migration through the regulation of RhoA activation. Genes Dev. *18*, 862–876.

Bortner, D.M., and Rosenberg, M.P. (1997). Induction of mammary gland hyperplasia and carcinomas in transgenic mice expressing human cyclin E. Mol. Cell. Biol. *17*, 453–459.

Botz, J., Zerfass-Thome, K., Spitkovsky, D., Delius, H., Vogt, B., Eilers, M., Hatzigeorgiou, A., and Jansen-Durr, P. (1996). Cell cycle regulation of the murine cyclin E gene depends on an E2F binding site in the promoter. Mol. Cell. Biol. *16*, 3401–3409.

Calhoun, E.S., Jones, J.B., Ashfaq, R., Adsay, V., Baker, S.J., Valentine, V., Hempen, P.M., Hilgers, W., Yeo, C.J., Hruban, R.H., and Kern, S.E. (2003). BRAF and FBXW7 (CDC4, FBW7, AGO, SEL10) mutations in distinct subsets of pancreatic cancer: potential therapeutic targets. Am. J. Pathol. *163*, 1255–1260.

Chung, Y.J., Jonkers, J., Kitson, H., Fiegler, H., Humphray, S., Scott, C., Hunt, S., Yu, Y., Nishijima, I., Velds, A., et al. (2004). A whole-genome mouse BAC microarray with 1-Mb resolution for analysis of DNA copy number changes by array comparative genomic hybridization. Genome Res. *14*, 188–196.

Clurman, B.E., Sheaff, R.J., Thress, K., Groudine, M., and Roberts, J.M. (1996). Turnover of cyclin E by the ubiquitin-proteasome pathway is regulated by cdk2 binding and cyclin phosphorylation. Genes Dev. *10*, 1979–1990.

Deng, C., Zhang, P., Harper, J.W., Elledge, S.J., and Leder, P. (1995). Mice lacking p21CIP1/WAF1 undergo normal development, but are defective in G1 checkpoint control. Cell *82*, 675–684.

Dong, Y., Sui, L., Tai, Y., Sugimoto, K., Hirao, T., and Tokuda, M. (2000). Prognostic significance of cyclin E overexpression in laryngeal squamous cell carcinomas. Clin. Cancer Res. *6*, 4253–4258.

Ekholm-Reed, S., Mendez, J., Tedesco, D., Zetterberg, A., Stillman, B., and Reed, S.I. (2004). Deregulation of cyclin E in human cells interferes with prereplication complex assembly. J. Cell Biol. *165*, 789–800.

Firpo, E.J., Koff, A., Solomon, M.J., and Roberts, J.M. (1994). Inactivation of a Cdk2 inhibitor during interleukin 2-induced proliferation of human T lymphocytes. Mol. Cell. Biol. *14*, 4889–4901.

Fukuse, T., Hirata, T., Naiki, H., Hitomi, S., and Wada, H. (2000). Prognostic significance of cyclin E overexpression in resected non-small cell lung cancer. Cancer Res. *60*, 242–244.

Geng, Y., Eaton, E.N., Picon, M., Roberts, J.M., Lundberg, A.S., Gifford, A., Sardet, C., and Weinberg, R.A. (1996). Regulation of cyclin E transcription by E2Fs and retinoblastoma protein. Oncogene *12*, 1173–1180.

Geng, Y., Yu, Q., Sicinska, E., Das, M., Schneider, J.E., Bhattacharya, S., Rideout, W.M., Bronson, R.T., Gardner, H., and Sicinski, P. (2003). Cyclin E ablation in the mouse. Cell *114*, 431–443.

Giaccia, A.J., and Kastan, M.B. (1998). The complexity of p53 modulation: emerging patterns from divergent signals. Genes Dev. *12*, 2973–2983.

Hwang, H., and Clurman, B. (2005). Cyclin E in normal and neoplastic cell cycles. Oncogene *24*, 2776–2786.

Johnson, L., Mercer, K., Greenbaum, D., Bronson, R.T., Crowley, D., Tuveson, D.A., and Jacks, T. (2001). Somatic activation of the K-ras oncogene causes early onset lung cancer in mice. Nature *410*, 1111–1116.

Keyomarsi, K., Tucker, S.L., Buchholz, T.A., Callister, M., Ding, Y., Hortobagyi, G.N., Bedrosian, I., Knickerbocker, C., Toyofuku, W., Lowe, M., et al. (2002). Cyclin E and survival in patients with breast cancer. N. Engl. J. Med. *347*, 1566–1575.

Koepp, D.M., Schaefer, L.K., Ye, X., Keyomarsi, K., Chu, C., Harper, J.W., and Elledge, S.J. (2001). Phosphorylation-dependent ubiquitination of cyclin E by the SCFFbw7 ubiquitin ligase. Science *294*, 173–177.

Koff, A., Giordano, A., Desai, D., Yamashita, K., Harper, J.W., Elledge, S., Nishimoto, T., Morgan, D.O., Franza, B.R., and Roberts, J.M. (1992). Formation and activation of a cyclin E-cdk2 complex during the G1 phase of the human cell cycle. Science *257*, 1689–1694.

Loo, L.W., Grove, D.I., Williams, E.M., Neal, C.L., Cousens, L.A., Schubert, E.L., Holcomb, I.N., Massa, H.F., Glogovac, J., Li, C.I., et al. (2004). Array comparative genomic hybridization analysis of genomic alterations in breast cancer subtypes. Cancer Res. *64*, 8541–8549.

Malek, N.P., Sundberg, H., McGrew, S., Nakayama, K., Kyriakides, T.R., Roberts, J.M., and Kyriakidis, T.R. (2001). A mouse knock-in model exposes

sequential proteolytic pathways that regulate p27Kip1 in G1 and S phase. Nature *413*, 323–327.

Mao, J.H., Perez-Losada, J., Wu, D., Delrosario, R., Tsunematsu, R., Nakayama, K.I., Brown, K., Bryson, S., and Balmain, A. (2004). Fbxw7/Cdc4 is a p53-dependent, haploinsufficient tumour suppressor gene. Nature *432*, 775–779.

Minella, A.C., Swanger, J., Bryant, E., Welcker, M., Hwang, H., and Clurman, B.E. (2002). p53 and p21 form an inducible barrier that protects cells against cyclin E-cdk2 deregulation. Curr. Biol. *12*, 1817–1827.

Moberg, K.H., Bell, D.W., Wahrer, D.C., Haber, D.A., and Hariharan, I.K. (2001). Archipelago regulates Cyclin E levels in Drosophila and is mutated in human cancer cell lines. Nature *413*, 311–316.

Nateri, A.S., Riera-Sans, L., Da Costa, C., and Behrens, A. (2004). The ubiquitin ligase SCFFbw7 antagonizes apoptotic JNK signaling. Science *303*, 1374–1378.

Ohtani, K., DeGregori, J., and Nevins, J.R. (1995). Regulation of the cyclin E gene by transcription factor E2F1. Proc. Natl. Acad. Sci. USA *92*, 12146–12150.

Ohtsubo, M., and Roberts, J.M. (1993). Cyclin-dependent regulation of G1 in mammalian fibroblasts. Science *259*, 1908–1912.

Orlicky, S., Tang, X., Willems, A., Tyers, M., and Sicheri, F. (2003). Structural basis for phosphodependent substrate selection and orientation by the SCFCdc4 ubiquitin ligase. Cell *112*, 243–256.

Parrinello, S., Samper, E., Krtolica, A., Goldstein, J., Melov, S., and Campisi, J. (2003). Oxygen sensitivity severely limits the replicative lifespan of murine fibroblasts. Nat. Cell Biol. *5*, 741–747.

Philipp-Staheli, J., Kim, K.H., Liggitt, D., Gurley, K.E., Longton, G., and Kemp, C.J. (2004). Distinct roles for p53, p27Kip1, and p21Cip1 during tumor development. Oncogene *23*, 905–913.

Porter, P.L., Malone, K.E., Heagerty, P.J., Alexander, G.M., Gatti, L.A., Firpo, E.J., Daling, J.R., and Roberts, J.M. (1997). Expression of cell-cycle regulators p27Kip1 and cyclin E, alone and in combination, correlate with survival in young breast cancer patients. Nat. Med. *3*, 222–225.

Rajagopalan, H., Jallepalli, P.V., Rago, C., Velculescu, V.E., Kinzler, K.W., Vogelstein, B., and Lengauer, C. (2004). Inactivation of hCDC4 can cause chromosomal instability. Nature *428*, 77–81.

Salamanca, F., and Armendares, S. (1974). C bands in human metaphase chromosomes treated by barium hydroxide. Ann. Genet. *17*, 135–136.

Seabright, M. (1971). A rapid banding technique for human chromosomes. Lancet *2*, 971–972.

Sherr, C.J., and Roberts, J.M. (1999). CDK inhibitors: positive and negative regulators of G1-phase progression. Genes Dev. *13*, 1501–1512.

Sherr, C.J., and Roberts, J.M. (2004). Living with or without cyclins and cyclin-dependent kinases. Genes Dev. *18*, 2699–2711.

Singer, J.D., Gurian-West, M., Clurman, B., and Roberts, J.M. (1999). Cullin-3 targets cyclin E for ubiquitination and controls S phase in mammalian cells. Genes Dev. *13*, 2375–2387.

Smith, L.L., Coller, H.A., and Roberts, J.M. (2003). Telomerase modulates expression of growth-controlling genes and enhances cell proliferation. Nat. Cell Biol. *5*, 474–479.

Spruck, C.H., Won, K.A., and Reed, S.I. (1999). Deregulated cyclin E induces chromosome instability. Nature *401*, 297–300.

Spruck, C.H., Strohmaier, H., Sangfelt, O., Muller, H.M., Hubalek, M., Muller-Holzner, E., Marth, C., Widschwendter, M., and Reed, S.I. (2002). hCDC4 gene mutations in endometrial cancer. Cancer Res. *62*, 4535–4539.

Strohmaier, H., Spruck, C.H., Kaiser, P., Won, K.A., Sangfelt, O., and Reed, S.I. (2001). Human F-box protein hCdc4 targets cyclin E for proteolysis and is mutated in a breast cancer cell line. Nature *413*, 316–322.

Tallquist, M.D., and Soriano, P. (2000). Epiblast-restricted Cre expression in MORE mice: a tool to distinguish embryonic vs. extra-embryonic gene function. Genesis *26*, 113–115.

Todaro, G.J., and Green, H. (1963). Quantitative studies of the growth of mouse embryo cells in culture and their development into established lines. J. Cell Biol. *17*, 299–313.

Welcker, M., Singer, J., Loeb, K.R., Grim, J., Bloecher, A., Gurien-West, M., Clurman, B.E., and Roberts, J.M. (2003). Multisite phosphorylation by Cdk2 and GSK3 controls cyclin E degradation. Mol. Cell *12*, 381–392.

Welcker, M., Orian, A., Jin, J., Grim, J.A., Harper, J.W., Eisenman, R.N., and Clurman, B.E. (2004). The Fbw7 tumor suppressor regulates glycogen synthase kinase 3 phosphorylation-dependent c-Myc protein degradation. Proc. Natl. Acad. Sci. USA *101*, 9085–9090.

Won, K.A., and Reed, S.I. (1996). Activation of cyclin E/CDK2 is coupled to site-specific autophosphorylation and ubiquitin-dependent degradation of cyclin E. EMBO J. *15*, 4182–4193.

Wu, G., Lyapina, S., Das, I., Li, J., Gurney, M., Pauley, A., Chui, I., Deshaies, R.J., and Kitajewski, J. (2001). SEL-10 is an inhibitor of notch signaling that targets notch for ubiquitin-mediated protein degradation. Mol. Cell. Biol. *21*, 7403–7415.

Ye, X., Nalepa, G., Welcker, M., Kessler, B., Spooner, E., Qin, J., Elledge, S.J., Clurman, B.E., and Harper, J.W. (2004). Recognition of phosphodegron motifs in human cyclin E by the SCF^{Fbw7} ubiquitin ligase. J. Biol. Chem. *279*, 50110–50119.